PHENOTYPIC PARAMETER EXTRACTION FOR WHEAT EARS BASED ON AN IMPROVED MASK-RCNN ALGORITHM

/

基于改进 Mask-RCNN 算法的麦穗表型参数提取

Ruyi ZHANG [1)], Zongwei JIA *[1)], Ruibin WANG[1)], Simin YAO[1)], Ju ZHANG[1)]

[1)] College of Information Science and Engineering, Shanxi Agricultural University, Taigu / China

Correspondence: Tel:+86-13835441286; E-mail: jiazw@sxau.edu.cn

DOI: https://doi.org/10.35633/inmateh-66-27

Keywords: *Mask-RCNN, wheat ear, phenotype, image segmentation, feature information extraction*

ABSTRACT

The acquisition of traditional wheat ear phenotypic parameters is labour intensive and subjective, and some trait parameters are difficult to measure, which greatly limits the progress of wheat ear research. To obtain the phenotypic parameters of wheat ears in batches at a low cost, this paper proposed a convenient and accurate method for extracting phenotypic parameters of wheat ears. First, three improvement directions were proposed based on the Mask Region-Convolutional Neural Network (Mask-RCNN) model. 1) To extract the multiscale features of wheat ears, a hierarchical residual link was constructed in a single residual block of the backbone network ResNet101 to obtain information on different sizes of receptive fields. 2) The feature pyramid network (FPN) was improved to increase the recognition accuracy of wheat ear edges through multiple two-way information flow sampling. 3) The mask evaluation mechanism was improved, specific network blocks were used to learn and predict the quality of the mask, and the detection of wheat ears and grains was performed by precise segmentation; an automatic extraction algorithm was designed for wheat ear phenotypic parameters based on the segmentation results to extract 22 phenotypic parameters. The experiments showed that the improved Mask-RCNN was superior to the existing model in the segmentation accuracy of wheat ears and grains; the parameters of wheat ear length, width, and number of grains extracted by the automatic extraction algorithm were close to the manual measurement values. This research meets the demand for automatic extraction of wheat ear phenotype data for large-scale quality testing and commercial breeding and has strong practicability.

摘要

传统麦穗表型参数获取劳动强度大，主观性强，且部分性状参数难以测量，很大程度上限制了麦穗研究的进展。为了能用低成本批量获取麦穗的表型参数，本文提出一种便捷且精准的麦穗表型特征参数提取方案。首先基于 Mask-RCNN 模型提出三种改进方向，1）为了提取麦穗多尺度特征，在主干网络 ResNet101 的单个残差块内构建分层残差类链接以获取不同大小感受野的信息；2）改进 FPN 金字塔网络，通过多次双向信息流采样提高麦穗边缘的识别精度；3）增加掩码评价机制，采用特定的网络块来学习和预测掩码的质量，最终实现对麦穗和籽粒的精准分割。然后针对分割结果设计一种麦穗表型参数自动提取算法，提取包含麦穗的成熟度信息、颜色、形状、空间等 22 个表型特征的参数。实验证明本文改进后的 Mask-RCNN 在麦穗与籽粒的分割精度上优于现有模型；麦穗表型参数自动提取算法提取的麦穗长、宽、籽粒个数的参数接近人工测量值，满足大规模质量检测和商业化育种对麦穗表型数据自动化提取的需求，具有较强的实用性。

INTRODUCTION

Cultivate adaptable wheat varieties to increase yield and the sustainability of crop production, and it is inseparable from the extraction of refined wheat phenotyping parameters. As the key to wheat yield, the phenotypic parameters of wheat ears are particularly important. They are the main focus of agricultural researchers. Ear feature extraction helps distinguish wheat varieties *(He et al., 2005; Panfilova et al., 2019)*, evaluate wheat ear quality *(Vavilova et al., 2017; Khan et al., 2020)*, research wheat resistance *(Li et al., 2017; Li et al., 2020)* and Forecast wheat yield *(Khan et al., 2021; Würschum et al., 2018)*. However, we currently rely on the visual inspection of field crops by experts to quantify the characteristics of wheat ear shape under nondestructive conditions. During this task, a large amount of work depends on the judgment of external characteristics such as shape, colour, and spatial layout.

[1] *Ruyi, Zhang, As. M.Agr. Stud.; Zongwei, Jia, Prof. MCS.; Ruibin, Wang, As. M.Agr. Stud.; Simin, Yao, As. M.Agr. Stud.; Ju, Zhang, As. M.Agr. Stud.;*

These characteristic values are difficult to directly quantify and describe. This has severely restricted the progress of scientific wheat research and the promotion of advanced production technology. Therefore, it is of great significance to quickly extract the phenotypic parameters of wheat ears in batches.

Image processing data acquisition technology, because of its low cost and low difficulty, has been widely used in wheat research *(Sadeghi et al., 2019; Alkhudaydi et al., 2019)*. Bi et al. *(2010)* calculated ear length by finding the main axis direction angle and rotation to calculate the length of the circumscribed rectangle and used corner detection to calculate the wheat awn feature parameters. Wang et al. *(2017)* selected an appropriate threshold to segment wheat based on the pixel characteristics of the ear image and then used the column data waveform characteristics of the corrected image to calculate the number of wheat ears. Lu et al. *(2016)* used the method of fitting the central curve of the main part of the wheat ear to calculate the length of the wheat ear and calculated the number of spikelets by passing the curve through the spikelet area and calculating the grey difference. However, the accuracy of these methods for wheat ear image extraction is not high, and this affects the acquisition of wheat ear phenotypic parameters. In recent years, due to its powerful data extraction capabilities, deep learning has become a promising tool for phenotypic data acquisition *(Tsaftaris et al., 2016; Eliceiri et al., 2016; King., 2007)*. Pound *(2017)* et al. marked the spikelets and the skeleton of potted wheat, constructed a network based on the hourglass model, and used heatmap regression to locate and count the spikelets, and the counting accuracy reached 99.66%. Wang *(2017)* et al. used the improved and efficient Det-D0 model to detect, count and analyse wheat ears, and the counting accuracy reached 94%.

In summary, current scholars have acquired some parameters of wheat ears, such as ear length, width, and number of spikelets *(Du et al., 2018; Wang et al., 2020)*. However, each method is limited in obtaining characteristics, and they cannot meet the various needs of agricultural researchers regarding the phenotypic characteristics of wheat ears.

This paper collects and compares a large number of wheat ears and finds that wheat ears of different varieties or the same variety in different environments have differences in the grain gap, the number of grains per unit area, and the distribution of grains. These characteristics are difficult to measure directly. They cannot be effectively used in wheat ear variety identification and quality inspection. In terms of ear appearance and morphology, researchers mainly focus on the detection of wheat ear problems such as pest prediction and morphological diagnosis *(Huang et al., 2014; Goyal et al., 2021)*. In large-scale planting, the effects of climate and moisture impact the grouting duration, and the impact on the yield of wheat if these effects are not treated in time is extensive *(Verman et al., 2015)*. The identification of the wheat ear growth period can help farmland managers irrigate and fertilize at the correct times, which is helpful for the planning of field management activities *(Yang et al., 2018; Kiss et al., 2014)*.

To achieve batched, accurate, and automatic acquisition of wheat ear maturity information and refined multiangle phenotypic indicators, this paper improves the Mask-RCNN model and designs an automatic extraction algorithm to determine wheat ear phenotype parameters. This precise extraction aims to meet the needs of large-scale selection and breeding.

MATERIALS AND METHODS

Experimental data

To ensure the diversity of the data and improve the applicability of the model, this paper uses data gathered from the wheat filling stage to just before the wheat ears are cut in the mature stage, that is, from 2021-05-12 to 2021-06-08; the data were collected randomly every 3 days for Shanxi Wheat ears in the experimental field outside the University of Agriculture, Dingxiang Fine Seed Field in Xinzhou City, and in Mengjiazhuang Village, Taigu District. During this period, 51 varieties of wheat and 578 wheat ears were collected. The wheat ears picked are sealed each time to prevent the grains from being lost during transportation. During imaging, a clip was used to hold the wheat so that the wheat was in a natural drooping state. A fixed-position Sony camera FDR-AX45 (with a resolution of 5044×3056 pixels) was used. One photo was taken from each of the four angles, and a total of 1064 pictures were taken.

The collected images were processed to meet the data requirements of the model. The data production process is as follows:

1) Labelme 's point annotation (CreatePolygons) was used to circle the overall outline of the ear and the side grain outline and generate a mask image.

2) To increase the training speed, the original image was trimmed and zoomed, and the image was adaptively zoomed to 512 × 512 pixels.

3) Data enhancement operations such as noise interference, colour jitter, contrast transformation, and random rotation were used for data augmentation. 4) According to the ratio of 7:2:1, the data set was randomly divided into a training set, validation set and test set.

Wheat ear segmentation model design based on Mask-RCNN

Basic network architecture

The premise of the accurate extraction of wheat ear phenotypic parameters is to achieve accurate pixel-level segmentation of wheat ears. For this reason, this article aims to address the problems of small wheat ears, high density, and serious awn occlusion. Based on these three goals, the Mask-RCNN model is improved. The overall block diagram of the network is shown in Figure 1. First, the backbone feature extraction network Res2Net101 and the feature pyramid network BFPN are used to obtain the feature layer, and then ROIAlign uses the feature layer to map the candidate frame ROI recommended by the Region Proposal Network，Region (RPN) into a fixed size feature map, and finally, the obtained feature map is classified and detected by branch and bound The box returns. Mask IoU Head optimizes the segmentation branch and obtains the segmentation map.

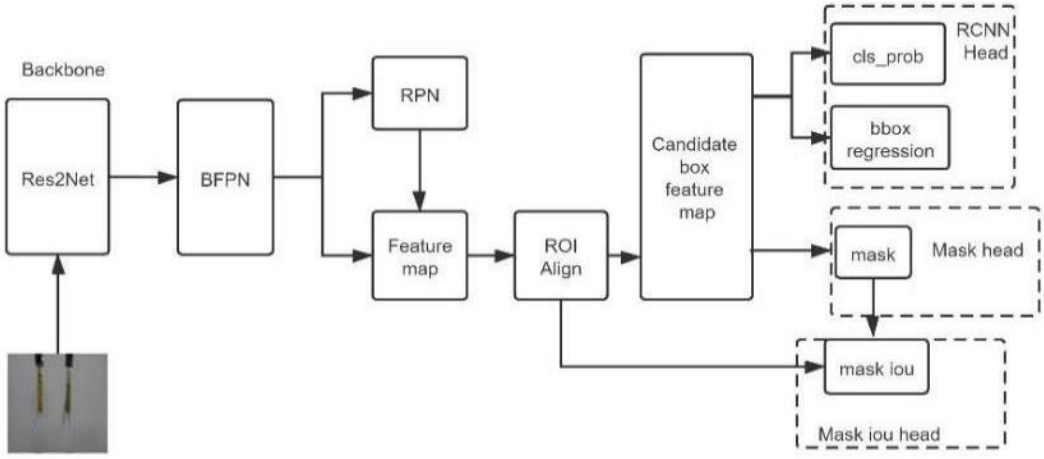

Fig. 1 - The overall block diagram of the improved algorithm based on Mask-RCNN

Feature extraction network design

The extraction of multiscale features is of great significance in computer vision, and designing a more effective structure can improve the ability of the network to extract features. In the process of identifying wheat ears and grains, due to the small grains and serious occlusion of wheat awns, missed inspections and faulty inspections can easily occur. More information is needed to express the characteristics of wheat ears. To improve the feature extraction capabilities of the network, this paper optimizes the backbone feature extraction network ResNet101 of Mask-RCNN and builds a hierarchical residual class link Res2Net module *(Gao et al., 2019)* in a single residual block in the residual network. Thereby improving the multi-scale representation ability at a more granular level, stronger multiscale characterization information under the same computing power is obtained. The structure is shown in Figure 2, and the network output can be expressed by equation (1).

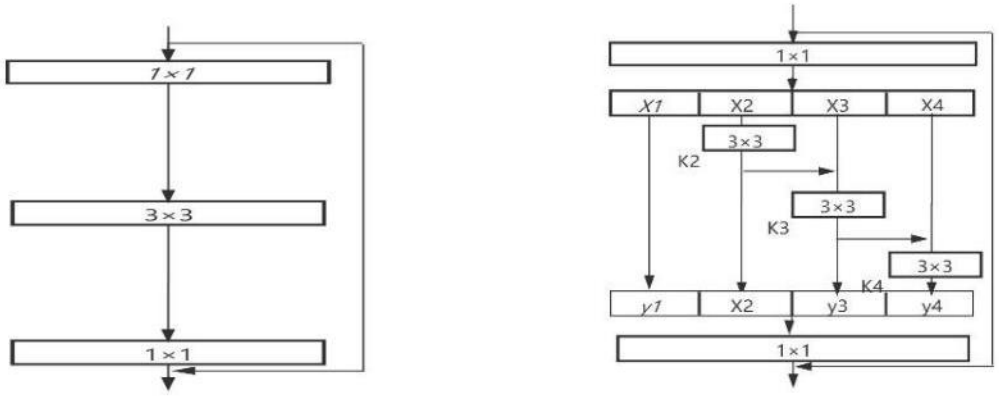

a. Bottleneck block b. Res2Net module

Fig. 2 - Res2Net structure

$$y_i = \begin{cases} x_i & \text{i=1} \\ k_i\left(x_i + y_i - 1\right) & 1<\text{i} \le \text{s} \end{cases} \quad (1)$$

The Res2Net module replaces the bottleneck block core of the residual block with multiple 3×3 filters and connects different filters in a hierarchical residual style. The connection form inside the module is similar to that of the residual network, and this helps to obtain different receptive field sizes. For example, y_2 will have a 3×3 receptive field, y_3 will have a 5×5 receptive field, and y_4 will have a larger size such as a 7×7 receptive field. In this way, the multiscale features of the granularity level are expressed, and the range of the receptive field of each network layer is increased. To increase the receptive field while reducing the computation as much as possible, omit the 3 × 3 convolutions, which can also be seen as the repeated use of a feature. In the replacement process, the hierarchical residual link does not increase the number of parameters, so it does not increase the burden on the network.

Design of the feature pyramid network (FPN)

In deep neural networks, shallow features pay more attention to detailed information, while high-level features pay more attention to semantic information. A traditional FPN combines high-level information upsampling with low-level features, which is essentially limited by one-way information flow. Only the high-level semantic information is enhanced, and the shallow semantic information of the neural network is highly correlated with detailed features such as edge shapes. The wheat ears and grains in this paper have serious adhesion, and the extraction of their characteristic parameters requires high edge accuracy. To fuse more features, this paper designs a multi-overlapped BFPN. Based on the unidirectional information flow of the original FPN, reverse downsampling information flow is added to fuse low-level edge features with high-level features to strengthen the extraction of the edge features of the wheat ears. The BFPN is shown in Figure 3.

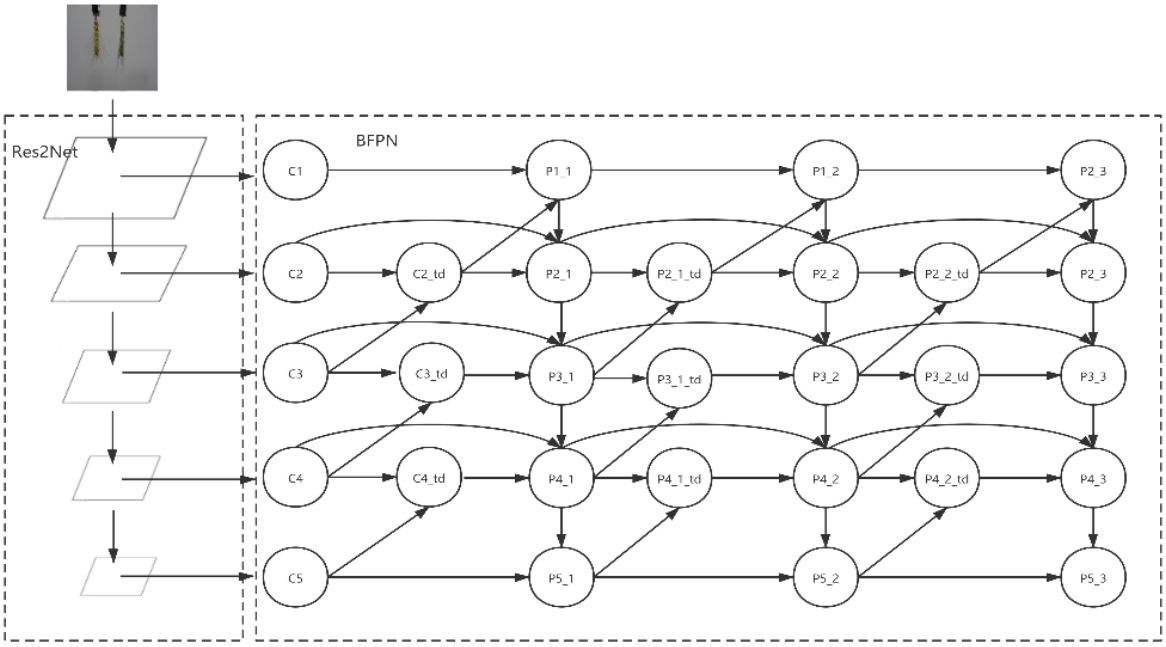

Note: The downward arrow indicates that convolution with a step size of 2 is used for downsampling, and the upward arrow indicates upsampling.

Fig. 3 - BFPN structure

To improve the fusion efficiency, this paper proposes several optimization methods for cross-scale connections. First, we remove the nodes that have only one input edge without feature fusion in the process of original FPN upsampling and shallow feature fusion to reduce the contribution of these nodes to feature fusion. The consumption of resources by small nodes is addressed. Second, when the shallow features are merged with the high-level features through downsampling, an extra edge (the feature layer ending with td in the figure) that is at the same level as the output node and has high-level information is added to fuse more features. Finally, each two-way path is regarded as a layer of the feature network, and the same feature network is stacked three times to obtain a higher level of scale fusion.

Improving the mask evaluation mechanism

In Mask-RCNN, the score of the mask branch is obtained based on the confidence of the classification branch. However, the mask quality usually does not have a high correlation with the classification score. If the score of the mask branch is used to evaluate the mask quality, there will be deviations. In this experiment, the segmentation mask determined based on the target detection classification frame of wheat ears is not the best segmentation structure, and it results in the low accuracy of the score for measuring the quality of wheat segmentation; the accuracy of the score will affect the performance of segmentation. To solve this mismatch problem, this paper adds a mask evaluation strategy, the Mask Scoring RCNN (*Huang et al., 2019*). Mask IoU Head is used to train the evaluation; it takes the features of the RoIAlign layer and the prediction mask together as input, completes the correct classification of the mask, and compares the prediction mask and the ground truth mask. The intersection over union (IoU) between the prediction mask and Mask IoU is used for regression to correct the deviation between the mask quality and mask score. The model in this paper also adds this part of the loss function to the model training. The structure is shown in the figure below, and the mask evaluation strategy is represented by:

$$Smask = Scls \cdot SIoU \tag{2}$$

$Scls$ represents the classification score, which focuses on the classification of the proposal, and represents the score of submission. $SIoU$ Focus on MaskIoU's regression.

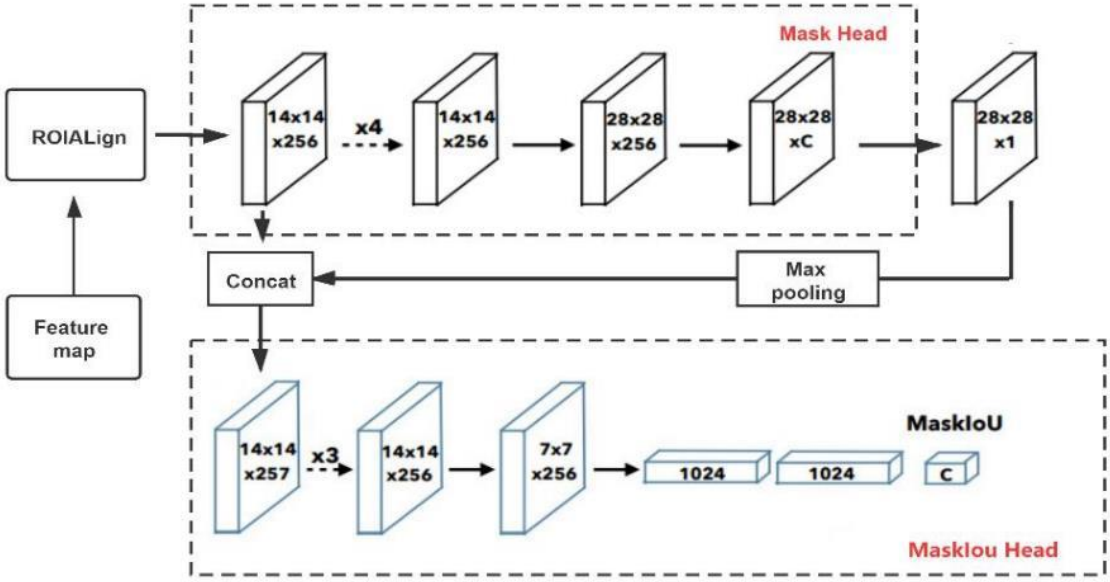

Fig. 4 - Structure diagram of the mask evaluation strategy

Design of the automatic extraction algorithm for wheat ear phenotypic parameters

Five kinds of mature wheat that do not exist in the training set or validation set, Jintai 188, Jintai 182, Zhongmai 175, Jingdong 22, and Chang 4738, were chosen as the test set, 3 plants of each wheat ear were selected, and images were taken from four angles. Finally, the improved Mask-RCNN model was used to segment the test set in real time, and the wheat ear phenotype parameters were obtained through the wheat ear phenotypic feature parameter extraction algorithm (as shown in Figure 5).

Table 1 describes the phenotypic characteristics of wheat ears. The feature extraction design is as follows:

1) Extraction of colour parameters. The wheat ear segmentation result is superimposed with the original image to separate the wheat ear, and the parameter values of the separated wheat ear are selected in the RGB three-colour space to represent the colour characteristics of the wheat ear.

2) Extraction of shape feature parameters. The camera calibration method is used to obtain the unit pixel length $\Delta\omega$, and the ear width and ear length are calculated by multiplying the unit pixel length by the maximum pixels in the vertical and horizontal directions of the wheat ear segmentation image. L is the ear length, W is the ear width, i is the i-th wheat ear, and n is the total number of wheat ears. Then, the average length and width of each ear are:

$$AvL = \frac{1}{n}\sum_{i=1}^{n} L_i \tag{3}$$

$$AvW = \frac{1}{n}\sum_{i=1}^{n} W_i \tag{4}$$

The average area is:

$$AVArea = \frac{1}{n}\sum_{i=1}^{n} \mathrm{CountAreamax} \times \Delta\omega^2 \tag{5}$$

The absolute error between the predicted value and true value is:

$$MAE = \frac{1}{n}\sum_{i=1}^{n} \left|\mathrm{GTi} - \mathrm{Prei}\right| \tag{6}$$

Through the results of grain segmentation, each grain on a single wheat ear can be separated, the phenotypic parameters of each grain can be extracted, and then the average value of the kernel parameters on a single wheat ear can be calculated. The number of grains is obtained by the return value of the mask, and the average area of all grains is $\overline{Areas}$:

$$\overline{Areas} = \frac{1}{r}\sum_{i=1}^{r} Areas_i \tag{7}$$

The average perimeter of the grain can be obtained in the same way. If the average value $\bar{x}$ is used, the standard deviation is:

$$\sigma = \sqrt{\frac{1}{r}\sum_{i=1}^{r} (x_i - \bar{x})} \tag{8}$$

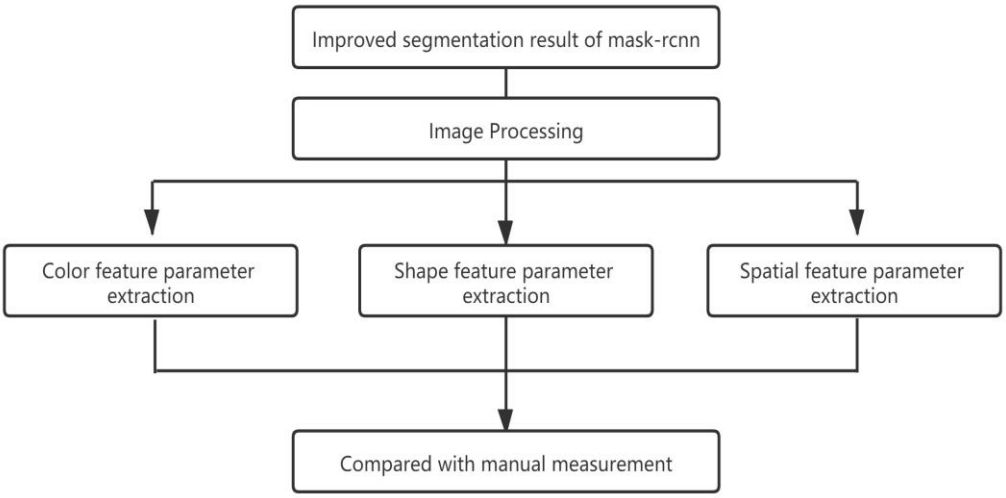

Fig. 5 - Flow chart of automatic extraction algorithm for wheat ear phenotypic parameters

3) Spatial parameter extraction. Spatial parameter extraction is performed jointly by the segmentation results of wheat ears and grains. The ear gap ratio is the ratio of the non-grain area to the entire wheat ear. The average grain angle calculation first derives the normal vector of the wheat ear according to the minimum circumscribed rectangle of the wheat ear mask and then calculates the angle of the grain through the wheat ear normal vector, as shown in Figure 6.

The gap distance between every two crystal grains in the same direction is obtained by the distance of the centre point of the smallest circumscribed rectangle of each crystal grain; then, the average gap distance $\bar{y}$ is:

$$\bar{y} = \frac{y}{r-2} \tag{9}$$

The grain density is closely related to the quantitative trait loci (QTL) mapping in wheat ρ (*Zhang et al., 2009*), and the number of grains per square metre is used to represent the grain density ρ:

$$\rho = \frac{r}{Area} \tag{10}$$

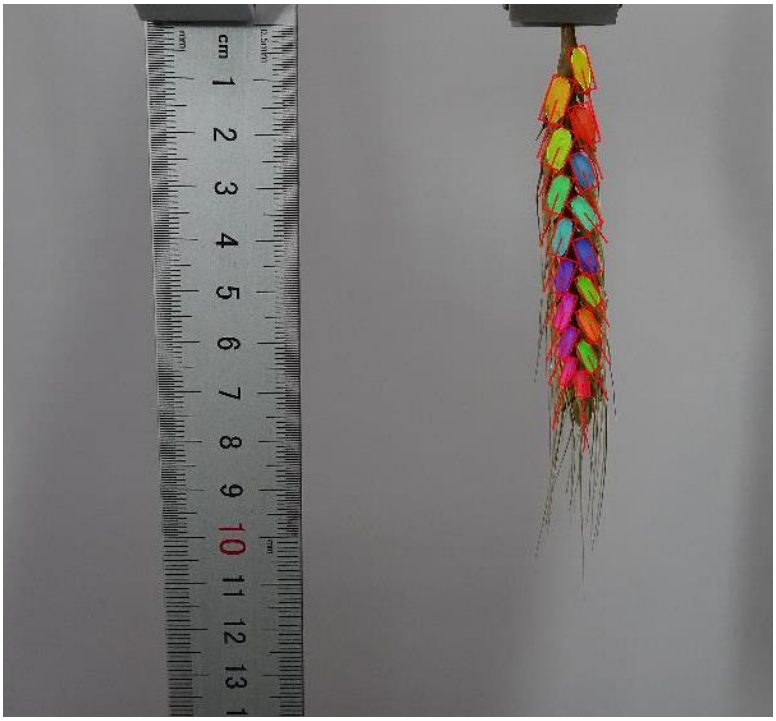

Fig. 6 - The diagram of Angle between grains

Table 1

Description of the wheat ear phenotype index

Types	Phenotyping indices	Description
period	maturity	The period in which wheat is grown or grated
Colour feature	R-channel mean	The red mean of RGB channels
	G-channel mean	The green mean of RGB channels
	B-channel mean	Average blue of RGB channels
Shape feature	Number of wheat ears/unit	The number of ears of wheat in the image
	spike length /cm	Maximum pixel length of the wheat ear in high direction
	ear width /cm	Maximum pixel length of the wheat ear in the broad direction
	panicle area /cm^2	The sum of the areas of the pixels occupied by wheat ears
	ear circumference /cm	Sum of pixel lengths of wheat fringe contour
	number of grains /pieces	The number of grains per ear on the image
	total grain area /cm2	Sum of pixel areas of all grains of a single wheat ear on the image
	Average grain area /cm2	Average pixel area of all grains of a single wheat ear on the image
	Standard deviation of grain area /cm	The standard deviation of a pixel area of all grains on a single ear of wheat on the image
	Average grain circumference /cm	Average pixel length of peripheral contour of all grains on a single wheat ear
	Standard deviation of grain circumference /cm	The standard deviation of pixel length of peripheral contour of all grains on a single wheat ear
Spatial feature	The proportion of ear gap /%	The ratio of non-grain pixel area of a single ear to the pixel area of the whole ear
	Kernel distance /cm	The mean pixel distance between the centre points of each pair of grains facing the same direction in a single ear
	Ear kernel distance standard deviation /cm	The standard deviation of gap length of a single ear
	Grain density /piece/cm2	The number of grains per square centimetre ear of wheat
	Grain density of the upper part /cm	The grain density of the upper part of the line is 1/2 the length of the ear
	Lower part grain density /cm	The grain density of the lower half of the line is 1/2 of the length of the ear
	Average ear grain Angle/^{o}	Taking the centreline of the wheat ear as the normal, the average Angle between the enclosing rectangle and the normal of all grains

RESULTS

Model comparison and analysis

To prove the effectiveness of the improvement, the Mask-RCNN model with a single improvement point was trained and tested in the same experimental environment. Improvement points 1-3 were adding the Res2Net module to the backbone network, improving the FPN, and adding the mask evaluation mechanism. The precision of the model after adding these improvement points is shown in the table 2 and 3. Each improvement point significantly improves the accuracy of wheat ear segmentation. The addition of the mask evaluation mechanism yields the most obvious improvement in accuracy, and the replacement of the backbone network has the least impact on the results. Compared with the original Mask-RCNN, the complete improved model increases 4.65 and 7.26 in the intersection ratios of wheat ear and grain segmentation, respectively; F1 increases 5.42 and 6.22, respectively.

Table 2

Mask-RCNN replacement of wheat ear segmentation accuracy comparison of different modules

Improvement Points of replacement	F1	Miou	Recall	Precision
No improvement	90.92	92.90	92.96	89.75
Improve the point 1	92.53	94.27	93.87	91.23
Improve the point 2	92.79	94.76	94.04	91.58
Improve the point 3	93.54	95.23	94.76	92.35
Improvement points 1, 2 and 3	96.34	96.74	97.21	95.48

Table 3

Mask-RCNN replacement of grain segmentation accuracy comparison of different modules

Improvement Points of replacement	F1	Miou	Recall	Precision
No improvement	90.92	92.90	92.96	89.75
Improve the point 1	92.53	94.27	93.87	91.23
Improve the point 2	92.79	94.76	94.04	91.58
Improve the point 3	93.54	95.23	94.76	92.35
Improvement points 1, 2 and 3	96.34	96.74	97.21	95.48

Figure 7 shows the same experimental environment; for UNet, DeepLabV3+, and Mask-RCNN, the network training process loss change map is displayed. For example, for the accuracy shown in Tables 4 and 5, the network loss value is lower than those of the existing models, reaching approximately 0.1. Mask-RCNN, UNet, and DeepLabV3+ are compared, and the recall, accuracy, F1 and mean IoU (miou) indicators of the proposed model are higher than those of the existing models.

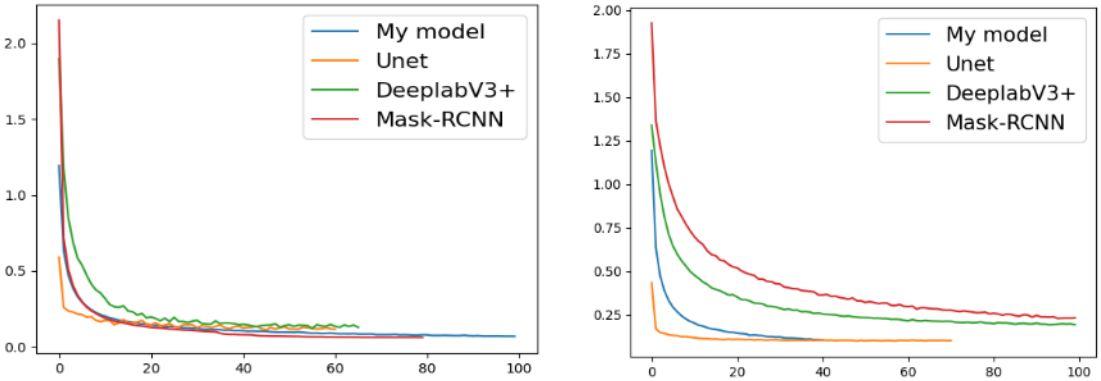

(a). Loss function curve of wheat ears *(b). Loss function curve of grains*

Fig. 7 - Training loss function curves of different models

Table 4

Comparison of wheat ear segmentation accuracy

Evaluation index	UNet	DeepLabV3+	Mask-RCNN	This model
Recall	91.35	90.15	92.96	97.21
Miou	90.31	89.98	92.90	96.74
Precision	90.21	88.67	89.75	95.48
F1	90.77	89.40	90.20	96.34

Table 5

Comparison of grains Segmentation Accuracy

Evaluation index	UNet	DeepLabV3+	Mask-RCNN	This model
Recall	81.60	76.31	79.64	85.09
Miou	81.40	73.25	81.41	88.67
Precision	74.30	65.45	80.31	87.34
F1	77.41	70.16	79.98	86.20

The segmentation results are shown in Figure 8. In the recognition of wheat, the UNet and DeepLabV3+ segmentation of the edge is rough, and the improved model can clearly recognize the edge details of wheat grains in identification. Since the target is a small grain that is densely distributed, UNet and DeepLabV3+ show inferior segmentation effects and multigrain adhesion. Mask-RCNN can identify each grain well, but the recognition of grain edge features is not sufficiently fine. Compared with the original model, the improved model can segment the grain more accurately.

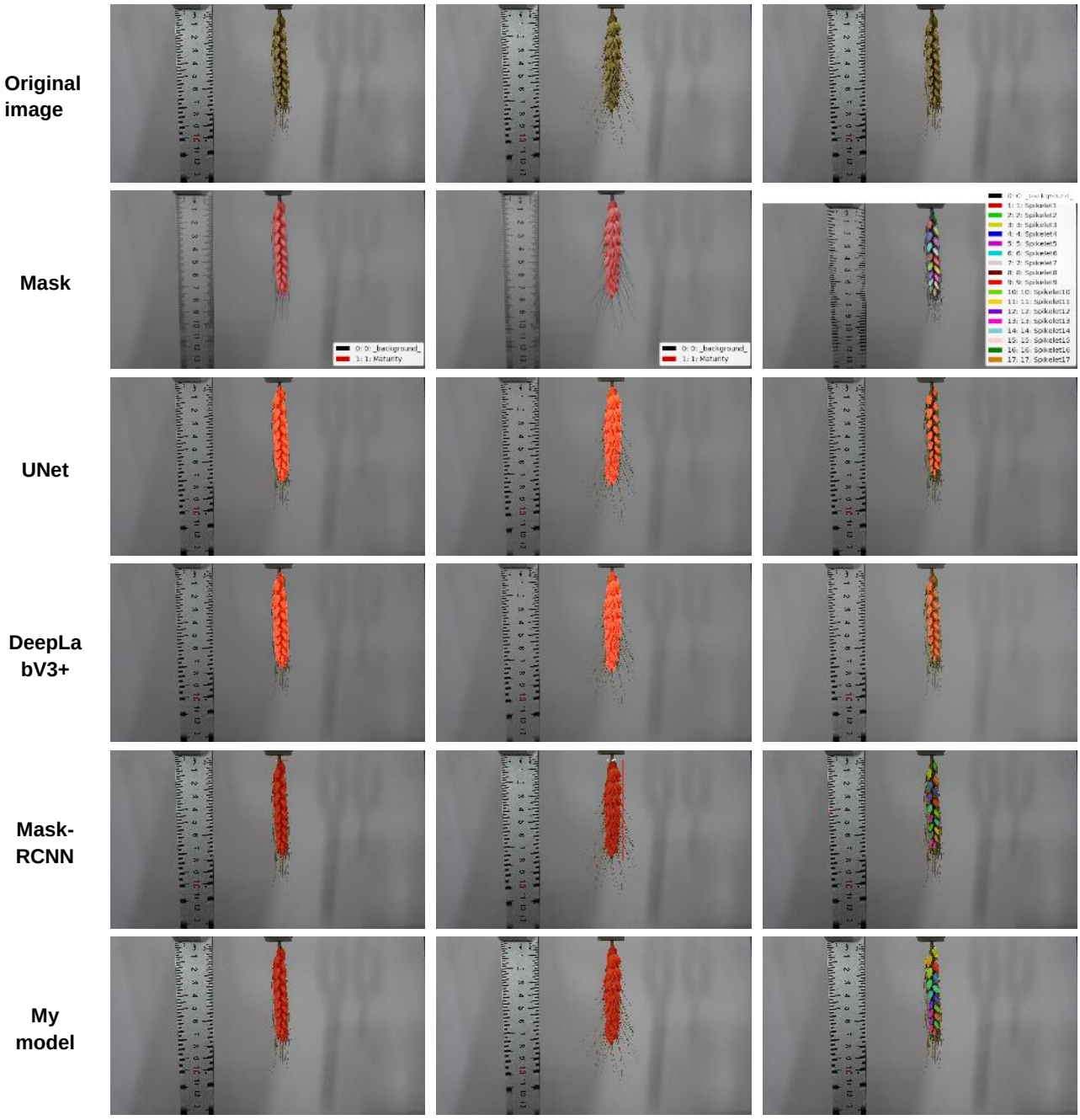

Fig. 8 - Prediction results of different models

Extraction of phenotypic parameters

The phenotypic parameters of wheat ears extracted using the scheme in this paper are shown in Table 6. The prediction of wheat ear maturity and the grains filling period in this scheme is consistent with the actual situation and has very high credibility. There are more or fewer differences in the phenotypic characteristics of different wheat varieties extracted by this scheme, which can provide technical support for the differentiation of wheat varieties and research on insect resistance. The Jintai188 and Zhongmai175 wheat grain density in the upper half are lower than that of the lower half of the grain density, and for Jintai188, the average grain angle is large, with more dispersed grain; for the Zhongmai175 wheat voids, the proportion is larger. Jintai182 is at a relatively high level in terms of length, width, and average grain size, while Jingdong22 is the opposite, with the smallest length, width, and average grain size.

Table 6

Wheat ear phenotypic parameters

Type	Phenotype	Jintai 188	Jintai 182	Zhongmai175	Jingdong22	Length 4738
period	maturity	mature stage	mature stage	mature stage	mature stage	mature stage
Colour feature	R-channel mean	2.01	3.52	2.41	1.97	2.71
	G-channel mean	1.73	3.11	2.07	1.69	2.37
	B-channel mean	0.92	1.58	1.17	1.01	1.36
Shape feature	Number of wheat ears /pieces	1	1	1	1	1
	Average spike length /cm	6.45	7.90	7.53	6.15	8.02
	Average ear width /cm	1.51	1.81	1.51	1.44	1.56
	Average panicle area /cm^2	5.62	8.75	7.26	5.23	7.8
	Average ear circumference /cm	14.60	18.27	14.14	14.18	18.02
	Average number of grains per seed/ pieces	17	17	17	15	17
	Average total grain area of a single ear /cm2	2.15	2.77	2.64	1.56	2.22
	Average grain area /cm2	0.13	0.16	0.156	0.10	0.13
	Standard deviation of grain area /cm	0.03	0.04	0.05	0.02	0.03
	Average grain circumference /cm	1.41	1.66	1.63	1.33	1.53
	Standard deviation of grain circumference /cm	0.21	0.19	0.26	0.19	0.19
Spatial feature	Average ratio of gap between ears /%	40.65	34.14	44.29	37.26	38.04
	Kernel distance /cm	1.65	2.49	1.61	1.54	2.00
	Ear kernel distance standard deviation /cm	1.01	1.96	1.29	1.19	1.57
	Grain density /cm2	3.21	2.09	2.84	3.57	2.93
	Grain density of the upper part /cm	3.02	2.22	2.68	3.80	3.10
	Lower part grain density /cm	3.40	1.96	3.02	3.22	2.74
	Average ear grain Angle /º	25.59	24.82	20.29	17.67	18.94

Table 7

The error between prediction results and manual measurement

Wheat types	Phenotype	Predicted mean	Measured mean	Error value
Jintai188	Length/cm	6.45	6.35	0.10
	Width/cm	1.51	1.45	0.06
	Number of grains/pieces	17	17	0
Jintai182	Length/cm	7.90	9.15	0.18
	Width/cm	1.81	1.90	0.09
	Number of grains/pieces	17	18	1
Zhongmai175	Length/cm	7.53	8.1	0.57
	Width/cm	1.51	1.40	0.11
	Number of grains/pieces	17	17	0
Jingdong22	Length/cm	6.15	6.45	0.30
	Width/cm	1.44	1.30	0.14
	Number of grains/pieces	15	15	0
Long4738	Length/cm	8.02	8.24	0.22
	Width/cm	1.56	1.40	0.16
	Number of grains/pieces	17	17	0

This model can quickly and concisely obtain the corresponding indicators of wheat ear colour, space and shape, but it is difficult to directly measure its parameters manually. The results for the features that can be manually measured by comparing them with the phenotypic parameters returned by the model in this paper are shown in Table 7. The model predicted values and measured values that are artificially strongly correlated by formula (6) can be obtained; the average length of all the wheat errors is 0.274 cm, the average width error is 0.112 cm, and the average error of the grain number is 0.2. The predicted value of the number of grains is basically the same as the actual value. Only one set of pictures has errors. The minimum measurement error of ear width is 0.06 cm, and the minimum error of ear length is 0.10 cm, which is close to the manual measurement value. The experimental results show that the method proposed in this paper has less error than manual measurement, and it can extract some indicators that cannot be directly measured manually while performing automatic extraction in batches.

CONCLUSIONS

In this paper, an automatic extraction scheme for wheat ear phenotypic characteristic parameters was designed to address the time consumption, limited extraction features, and low accuracy of the existing methods for obtaining wheat ear phenotypic characteristic parameters.

1) Aiming at the problems of awn of wheat severely occluded and grains adhesion in wheat ears, an improved Mask-RCNN model was used to segment wheat ears and grains; the Res2Net module was added to the backbone network of the original model to improve the multiscale feature extraction ability. Design a BFPN with 3 times superimposed two-way information flow instead of FPN network to enhance the edge recognition effect. Add the Mask IoU Head network, and improve the mask grading strategy. Finally, the contour of wheat ear segmentation is close to that of labelling, and the grain has clear edges with no adhesion.

2) Wheat ear phenotypic parameters were extracted based on the segmentation results. Aiming at the problem of limited extraction of wheat ear features by existing methods, an automatic extraction algorithm was designed for wheat ear phenotypic parameters. Extract 22 characteristics of wheat ears such as colour, shape, space, and maturity, including the length of the wheat ear, Among them, the index of ear length, width, and grain number are close to the artificial measurement values; other phenotypic index extraction methods can provide important technical support for research on wheat ear.

3) The proposed method can only be used to segment and extract characteristics of wheat ears and grains. The next step will be to study phenotypic extraction based on the number and length of wheat awns to improve the extraction of the phenotypic characteristic parameters of wheat ears.

ACKNOWLEDGEMENT

This work was supported by Shanxi Province Postgraduate Education Teaching Reform Project (2021YJJG087), Shanxi Province Educational Science "14th Five-Year Plan" Education Evaluation Special Project (PJ-21001) funded.

REFERENCES

[1] Alkhudaydi, T., Reynolds, D., Griffiths, S., Zhou, J., Iglesia, B. I. (2019). An exploration of deep-learning based phenotypic analysis to detect spike regions in field conditions for UK bread wheat. *Plant Phenomics*.

[2] Bi K., Jiang P., Li L., Shi B., Wang C., (2010). Non-destructive measurement of wheat spike characteristics based on morphological image processing. *Transactions of the CSAE*, 26 (12), 212-216.

[3] Du S., Li Y., Yao M., Li L., Ding S & He R., (2018). Grain counting method based on image segmentation of wheat spikes. *Journal of Nanjing Agricultural University,* 41(04), 742-751.

[4] Eliceiri, K.W., Berthold, M.R., Goldberg, I.G., Ibáñez, L., Manjunath, B. S., Martone, M. E., ... & Carpenter, A. E. (2012). Biological imaging software tools. *Nature methods*, *9*(7), 697-710.

[5] Goyal, L., Sharma, C. M., Singh, A., & Singh, P. K. (2021). Leaf and spike wheat disease detection & classification using an improved deep convolutional architecture. *Informatics in Medicine Unlocked*, 100642.

[6] Gao, S., Cheng, M. M., Zhao, K., Zhang, X. Y., Yang, M. H., & Torr, P. H. (2019). Res2net: A new multi-scale backbone architecture. *IEEE transactions on pattern analysis and machine intelligence*.

[7] He S., Li Z., He Z., (2005). Classification of wheat cultivar by digital image analysis. *Chinese Agricultural Sciences*, 38(09),1869-1875.

[8] Huang, Z., Huang, L., Gong, Y., Huang, C., & Wang, X. (2019). Mask scoring R-CNN. In *Proceedings of the IEEE/CVF Conference on Computer Vision and Pattern Recognition* , pp. 6409-6418.

[9] Khan, A. Q., Robe, B. L., & Girma, A. (2020). Evaluation of wheat genotypes (*Triticum aestivum L.*) for yield and yield characteristics under low land area at Arba Minch, Southern Ethiopia. *African Journal of Plant Science*, 14(12), 461-469.

[10] King, A. (2017). Technology: The future of agriculture. *Nature*, *544*(7651), S21-S23.

[11] Kiss, T., Balla, K., Bányai, J., Veisz, O., & Karsai, I. (2014). Effect of different sowing times on the plant developmental parameters of wheat (*Triticum aestivum L.*). *Cereal Research Communications*, *42*(2), 239-251.

[12] Li, Y., Li, H., Li, Y., & Zhang, S. (2017). Improving water-use efficiency by decreasing stomatal conductance and transpiration rate to maintain higher ear photosynthetic rate in drought-resistant wheat. *The Crop Journal*, 5(3), 231-239.

[13] Li, Y., Ma, L., Wu, P., Zhao, X., Chen, X., & Gao, X. (2020). Yield, yield attributes, and photosynthetic physiological characteristics of dryland wheat (*Triticum aestivum L.*)/maize *(Zea mays L.*) strip intercropping. *Field Crops Research*, 248, 107656.

[14] Lu Wenchao, Luo Bin, Pan Dayu, Zhao Yong & Wang C (2016). Synchronous measurement of wheat ear length and spikelets number based on image processing. *Journal of Chinese Agricultural Mechanization* (06), 210-215.

[15] Panfilova, A., Korkhova, M., Gamayunova, V., Drobitko, A., Nikonchuk, N., & Markova, N. (2019). *Formation of photosynthetic and grain yield of soft winter wheat (Triticum aestivum L.) depending on varietal characteristics and optimization of nutrition*.

[16] Pound, M. P., Atkinson, J. A., Wells, D. M., Pridmore, T. P., & French, A. P. (2017). Deep learning for multi-task plant phenotyping. In *Proceedings of the IEEE International Conference on Computer Vision Workshops* (pp. 2055-2063).

[17] Sadeghi-Tehran P., Virlet N., Ampe E. M. et al. DeepCount: in-field automatic quantification of wheat spikes using simple linear iterative clustering and deep convolutional neural networks [J]. *Frontiers in plant science*, 2019, 10: 1176.

[18] Tsaftaris, S. A., Minervini, M., & Scharr, H. (2016). Machine learning for plant phenotyping needs image processing. *Trends in plant science*, *21*(12), 989-991.

[19] Vavilova, V., Konopatskaia, I., Kuznetsova, A. E., Blinov, A., & Goncharov, N. P. (2017). DEP1 gene in wheat species with normal, compactoid and compact spikes. *BMC Genetics*, 18(1), 61-70.

[20] Verman, M. A. H. E. S. H., Jatav, S. K., & Gautam, A. (2015). Phenotypic stability analysis over different sowing times in wheat. *Annals of Plant and Soil Research*, *17*(3), 292-295.

[21] Wang, B., Lin, C., & Xiong, S. (2020). Wheat Phenotype Extraction via Adaptive Supervoxel Segmentation. In *2020 IEEE International Conference on Bioinformatics and Biomedicine (BIBM)*. pp. 807-814. IEEE.

[22] Wang N., Kong B., Wang C., Li W. & Xu H. (2017). Counting grains per wheat spike base in fractal segmentation of image. *Computer System& Applications* (10), 219-224.

[23] Wang, Y., Qin, Y., & Cui, J. (2021). Occlusion Robust Wheat Ear Counting Algorithm Based on Deep Learning. *Frontiers in Plant Science*, 12, 1139.

[24] Würschum T., Leiser W.L., Langer, S. M., Tucker, M. R., & Longin C.F.H. (2018). Phenotypic and genetic analysis of spike and kernel characteristics in wheat reveals long-term genetic trends of grain yield components. *Theoretical and Applied Genetics*, 131(10), 2071-2084.

[25] Yang, Y., Ding, J., Zhang, Y., Wu, J., Zhang, J., Pan, X., ... & He, F. (2018). Effects of tillage and mulching measures on soil moisture and temperature, photosynthetic characteristics and yield of winter wheat. *Agricultural Water Management*, *201*, 299-308.